

Wetting and reactivity in Ni–Si/C system: experiments versus model predictions

V. Bougiouri · R. Voytovych · O. Dezellus ·
N. Eustathopoulos

Received: 11 September 2006 / Accepted: 22 December 2006 / Published online: 21 February 2007
© Springer Science+Business Media, LLC 2007

Abstract Wetting of vitreous carbon C_v by NiSi alloys is studied in high vacuum using the sessile drop and dispensed drop techniques. The role of reactions between NiSi and C_v (simple dissolution or SiC formation) on wetting, adhesion and mechanical behaviour of the interface is determined and discussed. The experimental results on reactive wetting are compared with the predictions of two different approaches proposed recently in order to explain the thermodynamics and kinetics of this type of wetting.

Introduction

Metal matrix composites are generally processed by liquid state routes consisting of infiltration of the liquid metal into solid preforms or powders. There are two types of infiltration. If the liquid does not wet the solid (contact angle $\theta > 90^\circ$) infiltration must be performed using pressure to overcome the capillary pressure [1, 2]. In contrast, in wetting systems, spontaneous infiltration can occur. Molten silicon and Si-rich alloys wet carbon substrates [3, 4] and for this reason they can spontaneously infiltrate carbon preforms. *Reactive*

infiltration is used in practice to process SiC/alloy composites [5, 6] or the so-called “reaction bonded SiC” [7].

The objective of this study is to determine the wetting behaviour of NiSi alloys on flat, vitreous carbon substrates. The choice of this alloy was motivated by (i) the presence in the NiSi binary phase diagram of deep eutectics allowing a wide temperature range compatible with the experimental apparatus to be explored, (ii) knowledge of the physicochemical (surface tension) and thermodynamic properties (heat of mixing) of the liquid alloys needed in analysing the experimental results and (iii) knowledge of the ternary Ni–Si–C phase diagram [8]. In particular, Rado et al. [9] have shown that at temperatures in the 1,100–1,300 °C range with alloys containing more than $36(\pm 3)$ at% Si, Si reacts with carbon to form SiC, while with less Si the only reactivity between the alloy and carbon is some but limited carbon dissolution in the alloy. Note that Dezellus et al. reported elsewhere [10] the results of carbon wetting by a NiSi alloy containing 63 at% Si. The aim of the present study was to gain a complete picture of wetting and interfacial reactivity in the system by varying the alloy composition and temperature.

Experimental procedure

Wetting was studied both by the classical sessile drop technique and by the dispensed drop method, in a metallic furnace under a vacuum of $(1-7) \times 10^{-5}$ Pa. In the classical sessile drop experiment, nickel-silicon alloy droplets of 50–100 mg were prepared prior to the wetting experiment by melting pure Ni

V. Bougiouri · R. Voytovych · N. Eustathopoulos (✉)
SIMAP, ENSEEG, 1130 rue de la piscine,
38420 Saint Martin d'Hères Cedex, France
e-mail: nikos@ltpcm.inpg.fr

O. Dezellus
Université Claude Bernard Lyon 1,
LMI-UMR CNRS No 5615, 43 Bd du 11 novembre 1918,
69622 Villeurbanne Cedex, France

(99.997 wt%) and Si (99.9995 wt%) on pure alumina substrates in high vacuum. The wetting experiment consists in placing a piece of the alloy on a carbon substrate in the furnace at room temperature and then monitoring the changes in linear dimensions (drop base radius R and height) and contact angle θ of the drop during the continuous temperature rise and the subsequent isothermal hold, until steady contact angles are observed.

In the “dispensed drop” technique, the experiment involves heating Ni and Si in an alumina crucible placed above the carbon substrate. Once the experimental temperature is reached, the liquid is extruded from the crucible through a capillary and put in contact with the substrate. Thereafter, complete transfer of the drop to the substrate takes place and spreading continues as in the classical sessile drop configuration. This technique allows the process of melting and spreading to be separated so that fully isothermal experiments can be performed. Moreover during the extrusion process, any oxide skin on the liquid droplet is broken.

The wetting process is filmed by a video camera (25 frames per second) connected to a computer, enabling automatic image analysis. The characteristic dimensions of the drop (drop base radius R and contact angle θ) are extracted with an accuracy of $\pm 2^\circ$ for θ and $\pm 2\%$ for R . However the error on these quantities is higher ($\pm 4^\circ$ and $\pm 10\%$, respectively) in the case of contact angles in the 150° – 160° range [11].

Vitreous carbon substrates (V25 vitreous carbon) featuring no open porosity, an ash content of less than 50 ppm and a density of $1,500$ – $1,550 \text{ kg m}^{-3}$, were provided by Carbone-Lorraine, France. They were mechanically polished to a $1 \mu\text{m}$ diamond paste. The average roughness values R_a of the polished surfaces were 1 – 2 nm .

After cooling, selected specimens were cut perpendicularly to the interface: (i) the first half was embedded in resin and polished for optical and SEM observations and (ii) on the second part of the specimen, the metal droplet was dissolved using a $\text{HF} + \text{HNO}_3$ acid solution so as to reveal the interfacial area.

Results and discussion

Wetting of carbon by a non-reactive alloy

The first experiment was performed by the sessile drop technique at $1,217^\circ\text{C}$ for an alloy containing 21 at% Si, which, as noted in the Introduction, is non-reactive with carbon. After complete melting, a steady non-wetting contact angle $\theta_F = 123 \pm 3^\circ$ is established and remains constant in time. During cooling, thermal stress generated by differences in thermal contraction leads to detachment of the solidified droplet along the interface. SEM examination of the contact surfaces confirms the absence of an interfacial reaction compound. However, a depression of 20 – $30 \mu\text{m}$ was observed on the C_v substrate indicating carbon dissolution into the alloy. The non-wetting behaviour found here is not in agreement with certain results from the literature reviewed in [12–15], according to which the contact angle of pure Ni on carbon (and also of other ferrous metals not forming stable carbides such as Fe and Co) is much lower than 90° . A first possible reason for this discrepancy is that the value $\theta_F = 123 \pm 3^\circ$ is for a Ni–21 at% Si alloy, not for pure Ni. However, the thermodynamic activity of Si in this alloy is so weak (see Table 1) that the presence of this element has a very limited effect on the surface tension of Ni (about 5% for 21 at% Si) [17]. Another factor that has to be considered is the effect of dissolved carbon on the surface tension σ of Ni and NiSi alloys. However, as shown in Appendix, this effect is very limited (a few per cent).

In our opinion, the low wetting contact angles observed by some authors for pure Ni (and also pure Co and Fe) are due to the extensive dissolution of carbon into these metals occurring at temperatures of $1,500$ – $1,600^\circ\text{C}$. This leads to a macroscopically concave solid/liquid interface resulting in an apparent contact angle considerably lower than the true contact angle [12, 15]. This phenomenon is much less pronounced for the experiment described here, in which the relatively low experimental temperature and the presence of Si minimises carbon dissolution (see Appendix) so that the measured contact angle can be

Table 1 Experimental data obtained at $1,200^\circ\text{C}$ ($1,217^\circ$ for the 21 at% Si alloy)

	Si content (at%)	a_{Si}	Reactivity with C_v	θ_F ($^\circ$)	U^* ($\mu\text{m/s}$)	σ (J/m^2)	$\sigma_{\text{sl}} - \sigma_{\text{sv}}$ (J/m^2)
	66.8	0.49	R ^a	38	2.4	0.90	–0.71
	66.8	0.49	R ^a	36	2.8	0.90	–0.73
	57	0.3	R ^a	34	0.8	1.00	–0.83
	47	0.136	R ^a	20	0.4	1.15	–1.08
	21	0.001	NR ^b	123	-	1.68	0.91

The a_{Si} values are from [16]

^a Formation of SiC at the interface

^b Only carbon dissolution

considered as a good estimate of the Young contact angle of the system. It is interesting to note that the value $\theta_F = 123 \pm 3^\circ$ is close to (but somewhat lower than) the contact angles observed on C_v for the non-reactive Cu and Au (139° and 135° , respectively), dissolving negligible amounts of carbon. As argued in [18], adhesion in these systems is ensured by weak, Van der Waals interactions.

Reactive alloys: characteristic contact angles

A typical plot of drop base radius R and contact angle θ versus time for a dispensed drop experiment conducted at $1,200^\circ\text{C}$ with a Ni–66.8 at% Si alloy on vitreous carbon is given in Fig. 1a. Due to the rapid change in contact angle at the very beginning of wetting, more accurate determination of the behaviour of the contact angle θ in this domain is obtained using a logarithmic

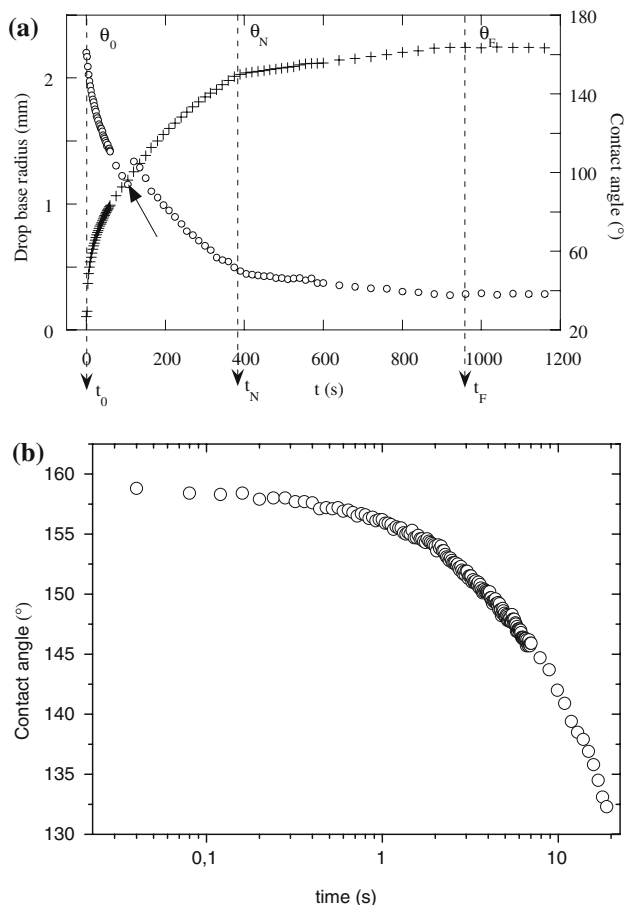


Fig. 1 (a) Contact angle and drop base radius versus time for a Ni–66.8 at% Si alloy at $1,200^\circ\text{C}$ by the dispensed drop technique. The perturbation on the $\theta(t)$ curve shown by an arrow corresponds to the moment of drop detachment from the capillary. (b) Logarithmic representation of θ versus time for $t < 20$ s

scale for time t as shown in Fig. 1b. According to this representation the contact angle tends in the range of very short times towards a constant value θ_0 close to 160° . Note that for such high contact angles the error on the absolute value of θ may be as high as $\pm 4^\circ$ (see the section “Experimental procedure”). However when a series of images is analysed by the same experimenter using the same method of image analysis, the relative error on the difference in θ values between two successive images is only $\pm 1^\circ$. This remark indicates that the plateau seen in Fig. 1b is an indisputable result. θ_0 values as high as 150° – 160° have already been observed in classical sessile drop experiments using various reactive metal–silicon alloys on vitreous carbon. These were identified as the contact angles of molten silicides on the unreacted C_v substrate [10]. The curve of Fig. 1b does not show a first, non-reactive spreading stage during which the contact angle decreases from 180° to θ_0 . Indeed, due to the very low viscosity of NiSi alloys (about $5\text{ mPa}\cdot\text{s}$ at $1,270^\circ\text{C}$ [19]), this stage is expected to be very fast, with a spreading time less than 20 ms , as for other metals and alloys [20–22]. As a consequence this stage cannot be observed by the camera used in the present study, which has a lower temporal resolution (40 ms).

The final contact angle $\theta_F = 36 \pm 2^\circ$ is much lower than the value close to 160° attributed to the unreacted NiSi/ C_v interface. Two different approaches have been proposed to explain the dramatic improvement in wetting observed in several reactive metal/ceramic systems. According to Landry and Eustathopoulos [23] both the final degree of wetting and spreading kinetics are controlled by the new compound formed at the interface. Conversely, Saiz et al. [24] pointed out that in many reactive cases the improvement in wetting is caused by adsorption of the reactive element at the alloy/initial substrate interface, and that frequently observed slow spreading rates and wetting hysteresis are often controlled by the dynamics of a triple line ridge. A first indication concerning the operating mechanism is given by the value $\theta_F = 36 \pm 2^\circ$, which is very close to the value $32.5 \pm 1.5^\circ$ measured previously for the same composition alloy on a single SiC crystal [9]. This strongly suggests that the final contact angle of the alloy on C_v is that on the SiC reaction layer. Indeed SEM observations and electron microprobe analysis (EMPA) of the interface performed on a cross-section showed that a SiC reaction layer was formed at the interface (Fig. 2). The thickness of the layer is 1 – $2\ \mu\text{m}$ at the centre of the interface and decreases to a few tens of nanometers at the triple line. There are three observations proving that the SiC layer formed during

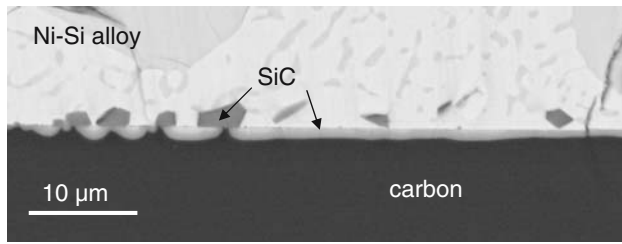


Fig. 2 SEM micrograph of a Ni–66.8 at% Si/C_v sample showing the transition of SiC microstructure from columnar (in the left part of the interface) to equiaxed (right). *T* = 1,200 °C, *t* = 49 min

spreading and not during cooling. (i) As for CuSi alloys on C_v [25], the SiC microstructure changes from equiaxed at the centre of the interface to columnar at the periphery, where the quasi-linear wetting was observed. (ii) If SiC was formed during cooling, by reaction between Si and C dissolved in the alloy, one would find SiC precipitates both close to and far from the interface. However SiC was found only at (or very close to) the interface, not in the bulk alloy. (iii) SEM observation of the triple line from above (Fig. 3) shows that in some places the triple line receded slightly during cooling from its initial position. One can clearly distinguish a reaction layer in the dewetted area, which, according to EDXS analysis, contains only carbon and silicon. From all these observations and results it is concluded that the improvement in wetting in the reactive system is due to the formation at the interface of wettable SiC and not to an adsorption phenomenon. Further evidence in favour of this mechanism is provided in the section concerning the effect of Si content.

Reactive alloys: spreading kinetics

The equilibrium contact angle was reached after a spreading time of 900 s. As observed in the case of Cu–Si alloys and pure silicon on vitreous carbon, two

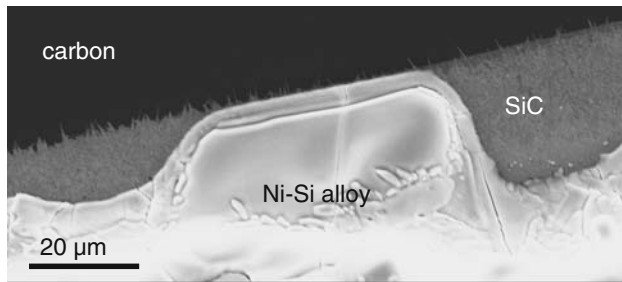


Fig. 3 SEM image of a triple line region of a Ni–66.8 at% Si alloy on C_v observed from above. X-ray micro-analysis of area exposed after receding reveals the presence of C and Si only

kinetic stages can be distinguished on the *R(t)* curve between *t*₀ ≈ 0 s and *t*_F (Fig. 1) [4, 10].

During most of the spreading kinetics (from *θ*₀ ≈ 160° to *θ*_N ≈ 50°), the spreading rate *U* = *dR/dt* decreases continuously and tends to a nearly constant value, noted *U*^{*}, when *θ* approaches *θ*_N. During this stage, the spreading kinetics are necessarily coupled to the reaction of SiC layer formation at the liquid alloy / carbon interface at the triple line. The fact that the spreading rate takes a nearly constant value *U*^{*} for the *θ* range from about 90° to 50° (Fig. 1) testifies that the spreading kinetics are not controlled by long-range diffusion of the reactive element (Si), but by the local reaction process at the triple line [10]. The second stage, during which the change in contact angle is very limited (about 15°), appears abruptly at *θ* = *θ*_N and is accompanied by a decrease in spreading rate by an order of magnitude. The origin of this stage will be discussed in a separate paper.

When the spreading rate is controlled by the local process at the triple line, the following equation was derived, according to which the cosine of the instantaneous contact angle varies exponentially with time [10]:

$$\cos \theta_F - \cos \theta = (\cos \theta_F - \cos \theta_0) \exp(-kt) \tag{1}$$

where *k* is a constant that can be related to the kinetic constant of the dissolution process *k*_d and to the driving force of the dissolution process *Δμ* by [26]:

$$k = k_d \frac{V_{SiC}^m}{f \cdot e} \Delta\mu \tag{2}$$

where *V*_{SiC}^m is the molar volume of SiC, *e* is the thickness of the reaction layer close to the triple line and *f* a geometrical factor of the order of unity [26]. The difference between the chemical potential of carbon in the solid and the liquid *Δμ* is related to the thermodynamic activity of Si in the alloy *a*_{Si} by the equation [26]:

$$\Delta\mu \approx RT \ln \left(\frac{a_{Si}}{a_{Si}^I} \right) \tag{3}$$

in which *a*_{Si}^I denotes the value of Si activity corresponding to the equilibrium of three phases: solid SiC, solid C and liquid alloy. Figure 4 shows a logarithmic plot of (cos *θ*_F – cos *θ*) as a function of time for *θ*_F = 32°. In the case of dispensed drop experiments, the perturbation of the *θ(t)* curves is due to drop detachment from the capillary, which leads to a sharp increase in the contact angle [10]. Note that the slopes of the straight lines before and after detachment were

observed to be the same, as expected for reaction-limited spreading (Fig. 4).

Effect of temperature

To evaluate the activation energy of reactive spreading in the quasi-linear stage, the constant k is determined for Ni-47 at% Si at three different experimental temperatures 1,150, 1,200 and 1,250 °C. Then, in order to obtain the true activation energy of the dissolution process, the logarithm of constant k divided by the driving force $\Delta\mu$ is plotted as a function of $1/T$ for Ni-47 at% Si liquid alloy in comparison with the results obtained earlier with Ni-63 at% Si [10] (Fig. 5). This assumes that all the other quantities (V_{SiC} , e) and factors (f) in Eq. 2 do not vary significantly with T .

The resulting activation energy values are 223 and 244 kJ mol⁻¹ for Ni-47 at% Si and Ni-63 at% Si alloys, respectively. Taking into account the above assumptions and the experimental errors, an effect of a_{Si} on the activation energy E_a can hardly be deduced and the value $E_a \approx 230$ kJ mol⁻¹ can represent the results for both alloys satisfactorily. In contrast, the results show a limited but significant effect of the Si activity on the value of the factor k_d and/or the reaction layer thickness e at the triple line. Note that a better evaluation of E_a would be possible if for each alloy the change with T of thickness e in the vicinity of the triple line was known. A systematic determination of e was not performed but it has been found, by profilometry applied to dewetted areas such as that shown in Fig. 3, that an increase in T of 100 °C causes an increase in e by a factor which would be at most

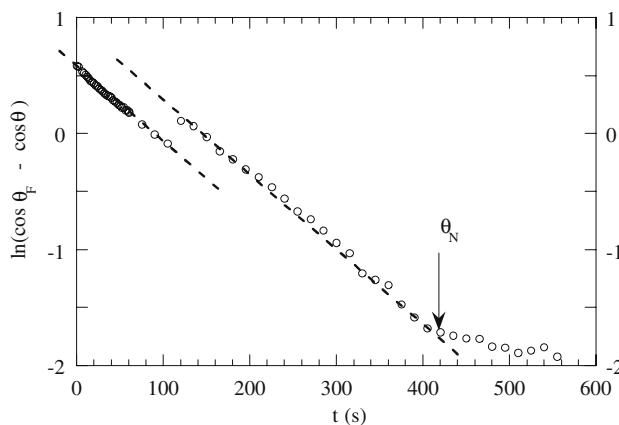


Fig. 4 Napierian logarithm of $\cos \theta_F - \cos \theta$ versus time t for Ni-66.8 at% Si alloy/ C_v system at 1,200 °C (dispensed drop technique). The arrow shows the time t_N at which the sharp change in the slope of the R versus t curves occurs (see Fig. 1). The vertical shift of the straight line at $t = 100$ s corresponds to the moment of drop detachment from the capillary

equal to 2. Such an effect of T on e would increase the activation energy by 45%. The value $E_a \approx 230$ kJ mol⁻¹ is one order of magnitude higher than the activation energies of diffusion in metallic melts (a few tens of kJ mol⁻¹). This confirms the conclusion drawn in the previous section that long-range diffusion in the liquid alloy does not limit the rate of spreading.

Effect of silicon content

The change in Si content in the alloy from 21 to 47 at% leads to a dramatic decrease, by nearly 100°, in the equilibrium contact angle (Table 1). This change corresponds to an increase of 2 J/m² in the difference (referred to as immersion energy [12]) $\sigma_{\text{sl}} - \sigma_{\text{sv}} = -\sigma \cos \theta_F$. This quantity, calculated for different reactive NiSi alloys on C_v from the values of θ_F of Table 1 and from values of σ in the literature, is plotted in Fig. 6 as a function of Si activity in the alloy. The values determined by Rado et al. [9] for the non-reactive system consisting of NiSi alloys on SiC substrates have been added in the same figure (the reason for the increasing values of $\sigma_{\text{sl}} - \sigma_{\text{sv}}$ on SiC with increasing Si activity is discussed in [9]). As can be seen, the agreement is excellent. This quantitative agreement confirms the conclusion drawn in the section “Reactive alloys: characteristic contact angles”, that the *non-wetting to wetting transition* observed between the non-reactive and the reactive alloys is due to the replacement at the interface of vitreous carbon by wettable SiC. In other words in the case of reactive alloys, when the wetting equilibrium is attained, the solid involved in the solid-liquid and solid-vapour interfaces is the reaction product. For comparison purposes, Fig. 6b reports the change in σ_{sl} with the

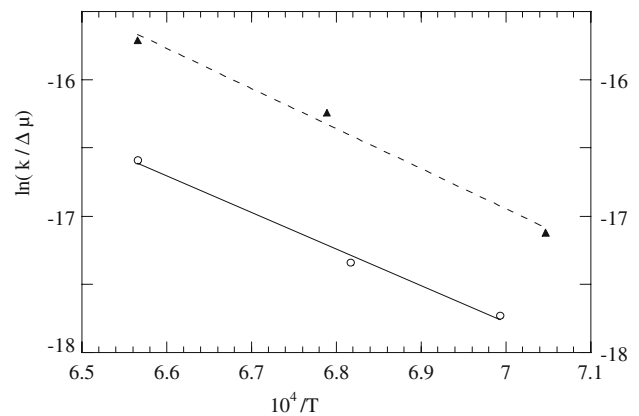


Fig. 5 Arrhenius plot of the reduced kinetic constant of dissolution $k/\Delta\mu$ for Ni-47 at% Si alloy (open circles) and for Ni-63 at% Si alloy (filled triangles)

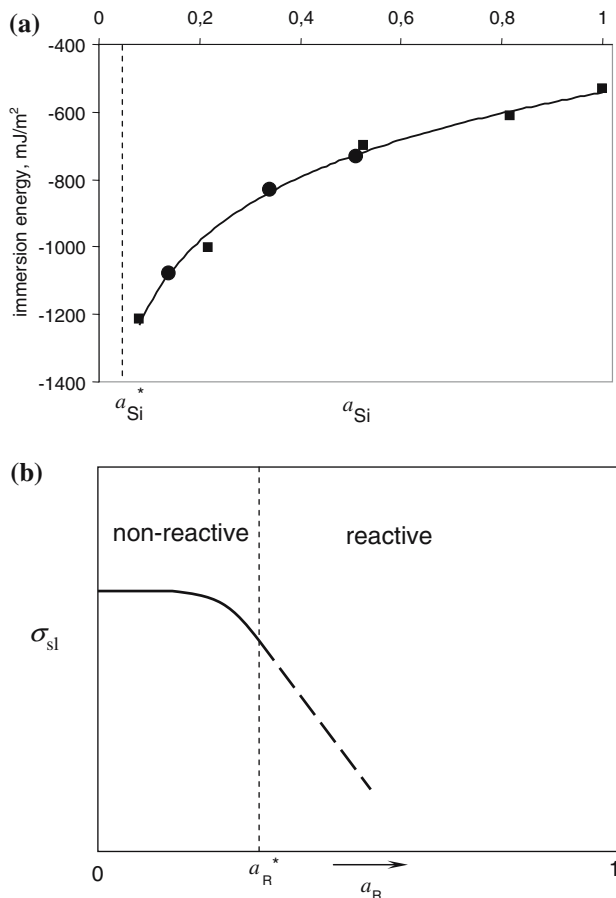


Fig. 6 (a) Immersion energy $\sigma_{\text{sl}} - \sigma_{\text{sv}}$ versus Si activity of NiSi alloys on C_v (circles, this study) and on SiC (squares, Rado et al. [9]). $T = 1,200$ °C. (b) σ_{sl} versus the activity a_R of a reactive solute R (schematic according to Saiz et al. [24]). In this case the interface considered is between the liquid and the initial substrate. a_R^* and a_{Si}^* are the activity values defining the transition from non-reactive to reactive alloys. Due to the scale used for the immersion energy, the value $\sigma_{\text{sl}} - \sigma_{\text{sv}} = + 910 \text{ mJ/m}^2$ obtained for the non-reactive alloy on C_v ($a_{\text{Si}} = 0.001$) is not in (a)

activity a_R of a reactive element R (here R is Si), as predicted by the approach of Saiz et al. The interface considered in this case is between the liquid and the initial substrate (here the vitreous carbon). Is the hypothesis of adsorption of Si at the alloy/ C_v interface compatible with the immersion energy values obtained on vitreous carbon with the non-reactive and reactive NiSi alloys? This would be true if the following two requirements were satisfied simultaneously: (i) Si must reduce, by adsorption, not only the alloy/ C_v interfacial energy but also the vitreous carbon–vapour surface energy and (ii) the resulting $\sigma_{\text{sl}} - \sigma_{\text{sv}}$ versus Si activity curve (where now $s = \text{C}_v$) must pass through a minimum at a molar fraction of Si lying between 0.21 and 0.47. Although not completely impossible, this schema is highly unlikely.

As has been noted before, the spreading rate U tends to a constant value U^* when θ approaches θ_N (Fig. 1). U^* values for different silicon contents are collected in Table 1.

If the quantities k_d and e in Eq. 2 do not depend (or depend only slightly) on a_{Si} , the spreading rate U^* will increase proportionally to the logarithm of silicon activity in the liquid (Eq. 3). The results of Table 1 qualitatively confirm this prediction. However, Eq. (2) underestimates the effect of a_{Si} . Thus for an increase of $\ln a_{\text{Si}}$ by a factor of 2.8, U^* increases by a factor of 6–7. This difference suggests that the assumption of k_d and e being a_{Si} -independent parameters is not completely valid.

Thermodynamic adhesion versus fracture energy

All the experiments performed with Ni–Si alloys containing from 47 to 67 at% Si led, after cooling, to cracking in the bulk of the carbon substrate. This behaviour attests that the interface in these cases is mechanically strong or, at least, stronger than bulk vitreous carbon. Conversely, in the case of the non-reactive Ni–21 at% Si alloy, brittle failure occurred at the alloy/carbon substrate interface, indicating that this interface is mechanically weak, corresponding to a low value of interfacial fracture energy Γ_i . In a metal/ceramic system, the value of Γ_i depends mainly on two parameters: (i) the yield stress of the metallic phase, reflecting the capability of the metal for energy dissipation by plastic deformation, and (ii) the intrinsic work of adhesion W_a of the metal on the ceramic, which is a good estimate of the energy of a perfect brittle failure. Although a precise expression of Γ_i as a function of W_a and the yield stress is not known, it is well established that Γ_i increases with increasing W_a and decreasing yield stress [27, 28].

As a general rule, metallic phases consisting only or mainly of intermetallics are brittle solids, having a negligible capability for energy dissipation by plastic deformation. Both the Ni–21 at% Si and Ni–47 at% Si alloys consist of intermetallic phase, so the dramatic difference in failure type observed between these two alloys can hardly be explained only by differences in the yield stress. The different failure behaviour is therefore likely to result to a great extent from differences in the values of the work of adhesion $W_a = \sigma (1 + \cos \theta_F)$, which can be calculated when the contact angle θ_F (Table 1) and the surface tension σ of the alloy are known [17]. For the Ni–21 at% Si alloy, a value of $W_a = 0.76 \text{ J/m}^2$ is found, while for the Ni–47 at% Si alloy $W_a = 2.23 \text{ J/m}^2$, which is three times higher. In order to study the relationship

between the thermodynamic adhesion parameters and the mechanical properties of the interface further, it is necessary to evaluate the properties by specific techniques, such as that presented in [29].

Conclusions

In the liquid NiSi/Cv system, reactivity depends critically on the molar fraction x_{Si} in the alloy. At low x_{Si} , reactivity consists in some but limited dissolution of carbon into the alloy. At high x_{Si} , Si reacts with C to form SiC layers of the order of a micron in thickness at the interface. The change in the type of alloy /substrate interface, from NiSi/Cv to NiSi/SiC, leads to a dramatic change in wetting (from contact angles much higher than 90° to contact angles in the $20\text{--}40^\circ$ range) and in work of adhesion (by a factor of 3) as well as in the mechanical response of the system to thermal stress (from interfacial failure to cohesive failure through the Cv substrate). The spreading rate is found to depend strongly on temperature (activation energy $\approx 230 \text{ kJ mol}^{-1}$) and on silicon activity in the alloy, indicating a reaction-controlled spreading process. The experimental results are in agreement with the approach to reactive wetting proposed in [23], according to which both the final degree of wetting and the spreading rate are controlled by the interfacial reaction product. Note that this conclusion is valid not only for carbon substrates. Indeed, a similar conclusion was drawn recently for an oxide ceramic (alumina) [30].

Appendix

The surface tension of C-saturated Ni at $1,350^\circ\text{C}$ (at this temperature molten Ni dissolves 8 at% of C [31]) is close to 1720 mN/m [15], while the surface tension of pure undercooled Ni at this temperature is $1,810 \text{ mN/m}$ [32]. This corresponds to an average decrease in σ of $10\text{--}15 \text{ mN/m}$ per 1 at% of dissolved carbon. Notice that the carbon concentration at saturation for the different Ni–Si alloys studied in this investigation (Table 1) is much less than 8 at% at temperatures close to $1,200^\circ\text{C}$. This is not only because the temperature is lower but especially because the addition of Si to Ni leads to a strong decrease in the solubility of carbon. Thus, according to [8] the solubility limit of carbon in a Ni–21 at% Si alloy at $1,200^\circ\text{C}$ is less than 2 at% while for a Ni–40 at% alloy this becomes lower than 0.5 at%. With such low C concentration values the effect of this element on the

surface tension of different Ni–Si alloys is expected to be very weak (a few percent), unless strong co-segregation of Si and C occurs at the Ni surface. Co-segregation of C and Si could be significant if the interactions between these elements in the liquid are strong. However, these interactions, expressed for the sake of simplicity using the parameter of sub-regular solutions $\lambda = \lambda_0 + aT$ (where λ_0 and a are constants) are very weak ($\lambda = +16 \text{ kJ/mol}$) compared with both Ni–C ($\lambda = -59 \text{ kJ/mol}$) and Ni–Si ($\lambda = -119 \text{ kJ/mol}$) [8]. We conclude that the use of Ni–Si surface tensions to calculate the immersion energy of NiSi alloys on Cv and SiC substrates (Fig. 6) is a very reasonable approximation.

References

- Mortensen A (2000) In: Comprehensive composite materials, Melt infiltration of metal matrix composites, vol 3. Pergamon, Oxford, p 521
- Alonso A, Pamies A, Narciso J, Garcia-Cordovilla C, Louis E (1993) Metal Trans A 24A:1423
- Whalen TJ, Anderson AT (1975) J Am Ceram Soc 58:396
- Dezellus O, Jaques S, Hodaj F, Eustathopoulos N (2005) J Mater Sci 40:2307
- Singh M, Behrendt DR (1994) J Mater Res 9:1701
- Messner R, Chiang YM (1990) J Am Ceram Soc 73:1193
- Hozer L, Lee JR, Chiang YM (1995) Mater Sci Eng A 195A:131
- Du Y, Schuster JC (1999) Met Mater Trans A 30A:2409
- Rado C, Kalogeropoulou S, Eustathopoulos N (1999) Acta Mater 47:461
- Dezellus O, Hodaj F, Eustathopoulos N (2002) Acta Mater 50:4741
- Eustathopoulos N, Sobczak N, Passerone A, Nogi K (2005) J Mater Sci 40:2271
- Eustathopoulos N, Nicholas M, Drevet B (1999) In: Wettability at high temperature. Pergamon Materials Series: vol 3. Pergamon, Oxford, UK
- Weisweiler W, Mahadevan V (1972) High Temperature High Pressure 4:27
- Naidich YV, Perevertailo VM, Nevodnik GM (1992) Poroshkovaya Metallurgiya 7:51
- Hara S, Nogi K, Ogino K (1995) In: Proceedings of the international conference on “high temperature capillarity”, Smolenice castle, May 1994, Bratislava, p 43
- An Mey S (1986) Z Metallkunde 77:805
- Keene BJ (1987) Surf Interface Anal 10:367
- Dezellus O, Eustathopoulos N (1999) Scripta Mater 40:1283
- Safonov SO, Ukhov VF, Vatolin NA (1972) Trudy Inst Met SverdI 98:27
- Naidich YV, Zabuga V, Perevertailo V (1992) Adgeziya Raspl Paika Mater (Rus) 27:23
- Ebril N, Durandet Y, Strezov L (2001) Trans JWRI 30:351
- Saiz E, Hwang CW, Sukanuma K, Tomsia AP (2003) Acta Mater 51:3185
- Landry K, Eustathopoulos N (1996) Acta Mater 44:3923
- Saiz E, Cannon R, Tomsia A (2000) Acta Mater 48:4449
- Dezellus O, Hodaj F, Rado C, Barbier JN, Eustathopoulos N (2002) Acta Mater 50:979

26. Dezellus O, Hodaj F, Eustathopoulos N (2003) *J Eur Ceram Soc* 23:2797
27. Reimanis I, Dagleish B, Evans A (1991) *Acta Metal Mater* 39:3133
28. Howe J (1993) *Int Mater Rev* 38:257
29. Sobczak N, Sobczak J, Nowak R, Kudyba A, Darlak P, Mikulowski B, Wojciechowski A (2005) *J Mater Sci* 40:2547
30. Voytovych R, Robaut F, Eustathopoulos N (2006) *Acta Mater* 54:2205
31. Massalski TB (ed) (1990) *Binary alloy phase diagrams*, 2nd edn. ASM International, Metals Park, Ohio
32. Brillo J, Egry I (2005) *J Mater Sci* 40:2213